RSC Advances

PAPER

Cite this: *RSC Adv.*, 2016, **6**, 110011

A green synthesis of Pd nanoparticles supported on modified montmorillonite using aqueous *Ocimum sanctum* leaf extract: a sustainable catalyst for hydrodechlorination of 4-chlorophenol†

Pallab Kumar Saikia,[a] Rakhi Paul Bhattacharjee,[ab] Podma Pollov Sarmah,[a] Lakshi Saikia*[a] and Dipak Kumar Dutta*[a]

Received 12th September 2016
Accepted 14th November 2016

DOI: 10.1039/c6ra22788k

www.rsc.org/advances

A green synthesis process in water has been developed with the aid of *Ocimun sanctum* (tulsi) leaf extract for the production of Pd nanoparticles (NPs) supported on modified montmorillonite. The leaf extract serves as a mild, natural and non-toxic reducing agent for converting the $K_2[PdCl_4]$ to Pd NPs. The synthesized Pd NPs were characterized by using PXRD, SEM, TEM, EDX, XPS, H_2-TPR and surface area analysis. TEM analysis reveals that particle sizes of the Pd NPs lie between a minimum of 10 nm and a maximum of 80 nm. The supported Pd NPs are used in the catalytic hydrodechlorination of toxic pollutant, 4-chlorophenol in water under base free conditions and showed conversion up to 98%. The catalyst is recoverable by filtration and could be recycled for several runs without any significant loss of catalytic efficiency.

1. Introduction

The synthesis of nanoparticulate materials and their applications as heterogeneous catalysts have received great attention because of their unique catalytic properties and robust catalyst stability.[1–8] The high surface area-to-volume ratio of metal nanoparticles provides a large number of available active sites for reaction per unit area which highly influence the catalytic activity. However, agglomeration of metal nanoparticles without support is inevitable, owing to their high surface energy, leading to a lowering of catalytic activity. In order to prevent agglomeration, considerable efforts have been made for development of suitable stabilizers or supports[9–11] which may play important role for controlling the particles size, morphology, distribution as well as the activity of the synthesized nanomaterials.[8–10] Controlled and precise growth of nanoparticles with the desired shape and size can be tuned by altering the morphology of the support. Recently, porous substances, like montmorillonite clay minerals, zeolites, charcoals containing nanosize channels, *etc.* have been used for the stabilization of metal nanoparticles.[12–18] From the prospective of advance catalyst design, the strategy of using an active support which helps in the reaction process is particularly attractive.[14,19] Montmorillonite belonging to the smectite group of clay may be considered as one such materials which is also environmentally benign. It possesses some unique properties such as cation exchange capacity, intercalation, swelling *etc.* which allow tuning its structural properties to be used as catalysts and catalysts supports.

In recent years, due to stringent and growing environmental regulations, the chemical industries need the development of eco friendly and sustainable synthetic methods for the synthesis of metal nanoparticles. The synthetic routes that use nontoxic solvents like water, reducing agents like biological extracts and microwave assisted synthesis *etc.* are becoming

Fig. 1 Image of *Ocimum sanctum* (tulsi) plant.

[a]*Materials Sciences and Technology Division, CSIR-North East Institute of Science and Technology, Jorhat 785006, Assam, India. E-mail: dipakkrdutta@yahoo.com; dutta_dk@rrljorhat.res.in; lsaikia@rrljorhat.res.in; Fax: +91 376 2370011*

[b]*Academy of Scientific & Innovative Research, Chennai 600113, India*

† Electronic supplementary information (ESI) available. See DOI: 10.1039/c6ra22788k

attractive.[20–24] Biosynthesis of NPs has several advantages over chemical synthesis from its simplicity, cost effectiveness, compatibility for biomedical and pharmaceutical application point of view.[25–28]

Ocimum sanctum, commonly known as tulsi, is a plant native to the Indian subcontinent and widespread as a cultivated plant throughout the Southeast Asian tropics [Fig. 1]. The leaves of this plant are rich in phenolic acids, flavonoids, propenyl phenols, terpenoids *etc.*[29,30] The bio-chemicals act as an excellent reducing agent that are easy accessible, nontoxic, cheap and environment friendly natural source of reductant for the synthesis of metal nanoparticles.

Chlorophenols (CPs) are present in waste water from paper, dyes, pesticides, textiles, and petrochemicals industries.[31–34] Among the CPs and other most harmful organic contaminants, 4-CP is considered as a hazardous pollutant because of its acute toxicity and strong bioaccumulation potential.[35] The presence of the stable chlorine–carbon bond in CPs made it difficult to biodegrade. Hence, to develop mild methods for dechlorination of CPs is of great importance. Among the different dechlorination techniques, catalytic hydrodechlorination (HDC) is considered as a suitable process for the treatment of wastewater containing organochlorinated pollutants.[36,37] Compared to other techniques, HDC has the advantages like, mild operating condition, converts the CPs to value added products which can be recovered and reused. In catalytic HDC, mainly supported or unsupported noble metals are used as the active phase but now-a-days supported bimetallic metal NPs are also extensively studied. Moreover, HDC is a structure-sensitive reaction,[38–42] hence designing catalysts with well-defined nanoparticles sizes and with uniform distribution is of great interest. In this regard the nanoporous supports also play an important role in designing the NPs of desired size.

The present work reports a green synthesis process of Pd NPs with particle size ranging from 10–80 nm using aqueous *Ocimum sanctum* leaf extract as a reducing agent supported on modified montmorillonite. The modification of montmorillonite is done in order to increase the surface area and also for generation of pores which can act as good support and stabilizer in the synthesis of metal nanoparticles. The synthesized NPs are used in the catalytic HDC of the hazardous pollutant 4-CP in water under base free and mild reaction conditions. This synthesized catalyst is of heterogeneous in nature and can be easily recovered and reused several times without any significant loss in its catalytic efficiency.

2. Experimental

2.1 Materials and methods

Bentonite (procured from Gujarat, India) containing quartz, iron oxide *etc.* as impurities was purified by sedimentation technique to collect the <2 μm fraction. The basal spacing (d_{001}) of the air dried sample was about 12.5 Å. The specific surface area determined by N_2 adsorption was 101 $m^2\ g^{-1}$. The analytical oxide composition of the bentonite determined was SiO_2: 49.42%; Al_2O_3: 20.02%; Fe_2O_3: 7.49%; MgO: 2.82%; CaO: 0.69%; loss on ignition (LOI): 17.51%; and others (Na_2O, K_2O and TiO_2): 2.05%. The purified clay (*i.e.* montmorillonite) is then treated with 4 M hydrochloric acid in order to increase the surface area by generating pores. Potassium tetrachloropalladate and 4-chlorophenol were purchased from Alfa Aesar, U.K. and were used as supplied.

Powder XRD spectra were recorded on a Rigaku, Ultima IV X-ray diffractometer of 2θ range 2–80° using Cu-Kα source (λ = 1.54 Å). Specific surface area, pore volume, average pore diameter were measured with the Autosorb-iQ (Quantachrome USA). Specific surface areas of the samples were measured by adsorption of nitrogen gas at 77 K and applying the Brunauer–Emmett–Teller (BET) calculation. Prior to adsorption, the samples were degassed at 200 °C for 3 h. Pore size distributions were derived from desorption isotherms using Barrett–Joyner–Halenda (BJH) method. TPD/TPR experiments were performed in Quantachrome "ChemBET Pulsar TPR/TPD instrument in a quartz U-tube using a TCD detector. The presence of surface acidity of the samples was qualitatively studied by temperature programmed desorption of ammonia (NH_3-TPD). Prior to ammonia sorption, the sample was outgased in a flow of pure N_2 at 200 °C for 2 h. Subsequently, the sample was saturated in a flow of NH_3 for about 30 min. Physically adsorbed ammonia was removed in a flow of helium at 800 °C for 1 h. Finally NH_3 desorption was carried out with a linear heating rate of 20 °C min^{-1}, in the temperature range of 50–700 °C under flow of pure helium. Temperature programmed reduction (TPR) of the sample was performed by taking 80 mg of the sample. The reducing gas was a mixture of 5 vol% H_2 in N_2, at a flow rate of 80 ml min^{-1}. The temperature was increased at a rate of 20 °C min^{-1} from 40 °C to 750 °C. Scanning electron microscopy (SEM) images were obtained using ZEISS, SIGMA instrument. The energy dispersive X-ray spectroscopy (EDX) and elemental dot mapping were obtained with OXFORD X-Max^N instrument. Prior to examination, the samples were coated with gold. Transmission electron microscopy (TEM) and high resolution transmission electron microscopy (HRTEM) images were recorded on a JEOL JEM-2011 electron microscope and the specimens were prepared by dispersing powdered samples in isopropyl alcohol, and placing them on a carbon coated copper grid and allowing them to dry. The Pd contents were determined by Inductively Coupled Plasma Atomic Emission Spectroscopy (ICP-AES) using Perkin Elmer, OPTIMA 2000 instrument. Samples taken during the reaction were analyzed with a Trace GC 700 series GC System (Thermo Scientific) coupled with a FID detector and capillary column.

2.2 Preparation of support

2% dispersion of 4 g purified powdered montmorillonite in 4 M hydrochloric acid was made in a round bottom flask. The resulting dispersion was then refluxed for 1.5 h. After cooling, the supernatant liquid was discarded and the activated montmorillonite was dialised with deionised water till the conductance of the water becomes nearly equal to that of deionised water. The resulting mass was dried in an air oven at 50 ± 5 °C and designated as AT-mont.

2.3 Preparation of TL extract

20 g of fresh tulsi leaves was washed with double distilled water and chopped well to small pieces. The chopped leaves were taken in a conical flask with 100 ml of double distilled water and heated at 60 °C for 1 h. The resulting mixture was allowed to cool to room temperature and filtered. The filtrate was collected in a glass bottle and stored at 4 °C. The filtrate was designated as TLE.

2.4 Preparation of palladium nanoparticles supported on AT-mont.

1.2 g powdered AT-mont. was taken in a 100 ml round bottom flask and 32 ml (1.2 mmol) aqueous solution of $K_2[PdCl_4]$ was added slowly under vigorous stirring condition. The stirring was continued for 6 h followed by evaporation to dryness of the whole dispersion in a rotary evaporator. 300 mg of the dried mass was then dispersed in 5 ml deionised water and to it was added 30 ml TLE as reducing agent under continuous stirring condition. The dispersion was then heated to 90 °C under stirring condition for 10 h and the colour changed from brown to black which indicates the reduction of Pd^{2+} to Pd^0. The black solid mass was then filtered using whatman 42 filter paper and washed repeatedly with distilled water and finally dried in a vacuum desiccator. The material thus prepared was designated as PdNP@AT-mont.

2.5 Catalytic hydrodechlorination of 4-chlorophenol

4-CP (1 mmol), H_2O [3 ml = 18 mmol (approx)] and 30 mg PdNP@AT-mont. were added and the reaction mixture was stirred at different temperatures for different time. In order to check the recyclability, the used catalyst was separated from the reaction mixture by filtration. The recovered catalyst was washed with acetone and dried in desiccator which thereby becomes ready for the second run. The same process was applied for reuse of the catalyst up to 5th run. On completion of the reaction, DCM is added to the mixture where the substrate and all the probable products are easily soluble. The water and DCM mixture is then separated using a separating funnel and sodium sulphate. The DCM part is then taken for GC analysis to identify and determine the conversion of reactants into products.

3. Results and discussion

3.1 Characterization of support

The PXRD analysis of the parent montmorillonite exhibited an intense basal reflection at 2θ value of 7.06° corresponding to a basal spacing of 12.5 Å [ESI: Fig. 1†]. After 1.5 h of acid activation, the intensity of basal reflection decreases which implies that the layered structure of the clay is disrupted. A low intense broad reflection of 2θ in the range 0–30° confirmed the formation of amorphous silica.[12] The AT-mont. shows micro- (<2 nm) and mesopores (2–50 nm) with average pore diameters ~3.4 nm, a high specific surface area up to 346 $m^2\ g^{-1}$ as compared to that of parent mont. (101 $m^2\ g^{-1}$), and specific pore volume of ~0.3 $cm^3\ g^{-1}$ [Table 1]. The N_2 sorption isotherm [ESI: Fig. 2†] was of type-IV with a H3 hysteresis loop at $P/P_0 \sim 0.4$–0.9, indicating a mesoporous solid. The increase of surface area as well as pore volume is due to the leaching of Al from the clay matrix during acid activation, which also introduced permanent porosity on the clay surface. The differential volumes *versus* pore diameter plot [ESI: Fig. 2† (inset)] indicated relatively narrow pore size distributions and these nano range pores can be advantageously utilized for the *in situ* synthesis of various metal nanoparticles.[8,19]

Table 1 Surface properties of AT-mont. and PdNP@AT-mont.

Samples	Surface properties of support/catalysts		
	BET surface area ($m^2\ g^{-1}$)	Average pore diameter (nm)	Pore volume ($cm^3\ g^{-1}$)
AT-mont.	423	3.81	0.346
PdNP@AT-mont. (fresh)	284	3.76	0.194
PdNP@AT-mont. (after 5th run)	195	3.79	0.194

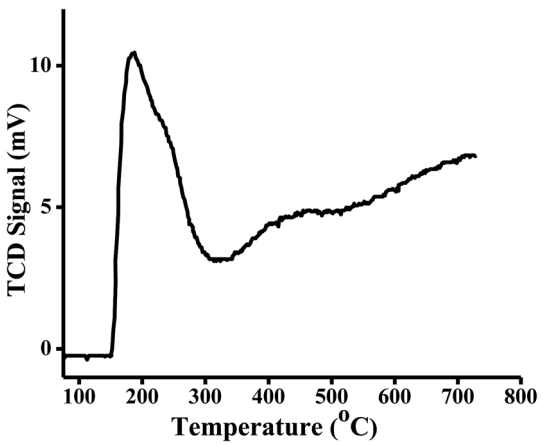

Fig. 2 NH_3-TPD profile of AT-mont. indicating the presence of different types of acid sites on the surface.

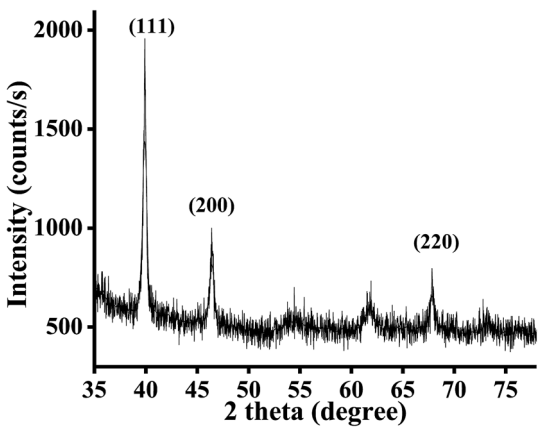

Fig. 3 PXRD spectra of PdNP@AT-mont. showing the different planes of Pd NPs.

The presence of the acid sites of the AT-mont. was qualitatively evaluated by thermal desorption of ammonia.[43] Ammonia, being a strong base, reacts even with extremely weak acid sites, which therefore makes NH_3-TPD a useful technique for evaluating the presence of acid sites on a surface. The acid strength of AT-mont. corresponded to a higher desorption temperature of NH_3 adsorbed on acid sites. The NH_3-TPD spectra of AT-mont. exhibits weak, medium and strong acid sites which are included in the region at 160–300 and 330–500 °C [Fig. 2]. The SEM image of AT-mont. [ESI: Fig. 3(a)†] showed the presence of layered structure and formation of pores on the clay surface. The EDX pattern of the surface [ESI: Fig. 3(b)†] revealed the presence of predominant amounts of Si compared to Al on the surface along with other elements of clay.

3.2 Characterization of PdNP@AT-mont.

Powder XRD analysis of Pd NP@AT-mont. [Fig. 3]. shows three peaks at 2θ values 40.1, 46.6 and 68.1 due to the (111), (200) and (220) indices of face centered cubic (fcc) lattice of metallic Pd.[44] Among the peaks observed, the intensity of (111) peak is the strongest, indicating that this plane was predominant crystal facet in PdNP@AT-mont. The incorporation of the Pd NPs into the nanopores of the AT-mont. has made a change in the textural parameters of the materials. The N_2-sorption analysis of the AT-mont. before loading and after loading [ESI: Fig. 4†] of the Pd NPs, shows the same type IV isotherm with a H3

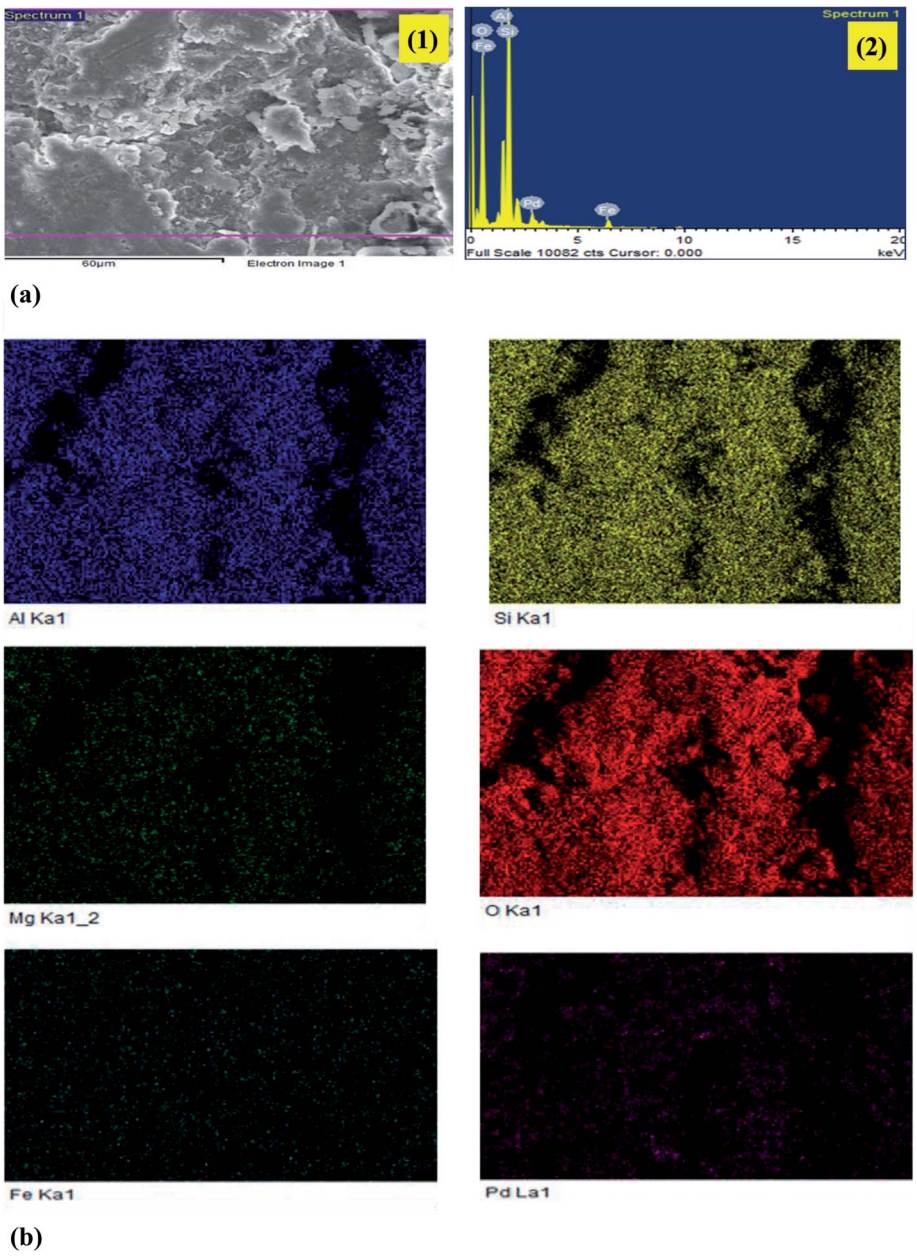

Fig. 4 (a) (1) SEM image and (2) EDX spectra of PdNP@AT-mont. (b) Elemental dot mapping of Al, Si, Mg, O, Fe and Pd on PdNP@AT-mont.

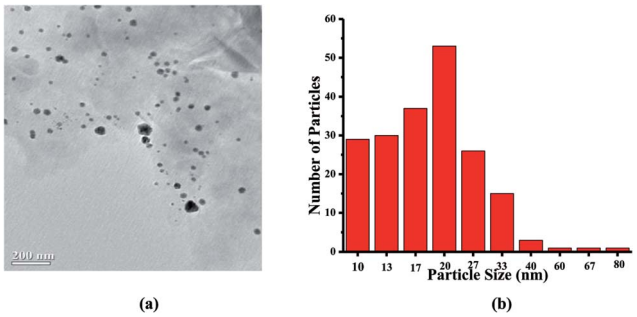

Fig. 5 (a) TEM image and (b) particle size distribution of PdNP@AT-mont.

hysteresis loop at $P/P_0 \sim 0.4$–0.9. This reveals that the ordered porous structure of clay exists even after the incorporation of Pd NPs. The BET surface area and total pore volume of AT-mont. decreased after the incorporation of Pd NPs [Table 1] which might be due to clogging of some pores by the Pd NPs. The absence of an abrupt change in the surface area and pore volume of the support after incorporation of Pd NPs also confirms that pores of the support are not blocked by Pd particles larger than the pore size of the support. This suggests that the well-tuned nanopores on the support materials do not allow the agglomeration of the NPs but instead stabilize or anchor them on the pore wall structure. In addition, the presence of Pd^0-nanoparticles may cause complexities in porosity measurement with N_2 sorption, because the electrostatic forces between an adsorbate (*i.e.* N_2) and metallic surface may affect the measured values to some extent.

The SEM and EDX analysis also substantiated the possible formation and the presence of Pd NPs on the well-tuned surface of the AT-mont. along with other elements of clay [Fig. 4(a)]. Furthermore, the elemental mapping [Fig. 4(b)] clearly indicates the presence and distribution of Pd along with other elements in the support. The TEM image of PdNP@AT-mont. [Fig. 5(a)] indicates that most Pd NPs are well distributed on the surface of AT-mont. and the particle size distribution histogram [Fig. 5(b)] reveals that there is a wide distribution of particles sizes from 10 to 80 nm. The XPS spectra [Fig. 6(a)] of Pd gives two peaks at 335.3 eV and 340.5 eV, which are the characteristic of Pd $3d_{5/2}$ and $3d_{3/2}$ respectively and corresponds to fully reduced Pd(0) NPs. The satellite peaks at 337.6 eV ($3d_{5/2}$) and 342.8 eV ($3d_{3/2}$) suggest the presence of some PdO particles.[44,45] The H_2-TPR profile for PdNP@AT-mont. [Fig. 6(b)] is characterized by the presence of a negative peak at 70–110 °C, which is related to the desorption of weakly adsorbed hydrogen from the Pd surface, and decomposition of the β-PdH_x phase formed at room temperature by diffusion of hydrogen into the Pd crystallites.[46] The reduction process observed in the temperature range 200–460 °C is attributed to the reduction of PdO particles, interacting strongly with the surface of the support.[47] This result shows that not all of the Pd(II) was reduced to Pd(0), which is probably due to the acidic environment of the TLE.[44,48] The residual palladium(II) should be easily reduced to palladium(0) in the catalytic hydrogenation reaction under hydrogen atmosphere. The Pd content in 100 mg of Pd NP@AT-mont. is found to be 8.14 mg.

3.3 Catalytic activity

The bio-synthesized PdNP@AT-mont. was investigated for the HDC of 4-CP at different temperatures in water under hydrogen balloon pressure and good to excellent conversions were obtained [Table 2]. The efficiency of the catalyst for HDC of 4-CP with respect to time and temperature were also studied. In all the cases, only phenol was found as the HDC product. HDC is a size sensitive reaction in which NPs of sizes around 3.5–6 nm were reported to show best results.[39,40,49] However, in the present study with particle sizes of catalyst greater than 10 nm also showed comparative results with extended reaction time and

Table 2 Catalytic HDC of 4-CP using PdNP@AT-mont. in water and H_2 balloon pressure at different temperature and time[a]

Sl no.	Temperature (°C)	Time (h)	Conversion[b] (%)	Selectivity (%)
1	Room temp.	7	50	100
2	40	6	96	100
3	50	5	86	100
4	60	5	92	100
5	70	4	98	100
6	80	3	97	100

[a] Substrates: 4-CP – 0.5 mmol, H_2O – 2 ml, PdNP@AT-mont. – 20 mg. [b] GC analysis.

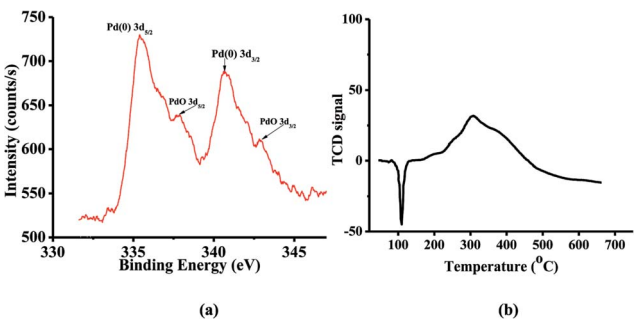

Fig. 6 (a) XPS spectra of PdNP@AT-mont. showing the presence of Pd(0) with formation of PdO and (b) H_2-TPR of PdNP@AT-mont.

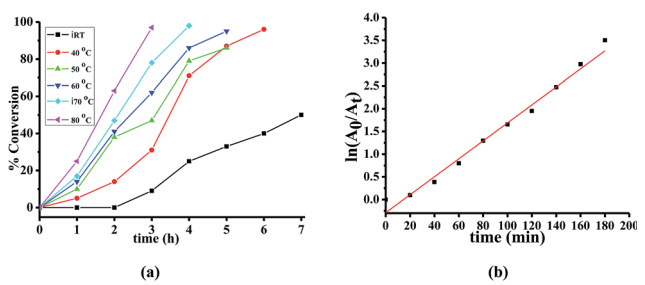

Fig. 7 (a) Pattern of progress HDC of 4-CP with time at different temperature and (b) the dynamics of HDC of 4-CP at 80 °C.

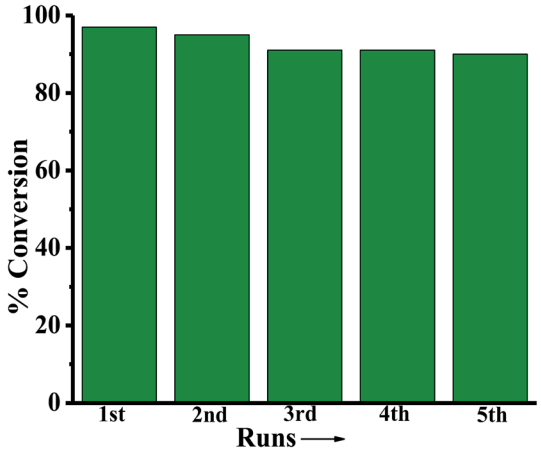

Fig. 8 Bar diagram showing the conversion of 4-CP up to 5th run of the recovered catalyst.

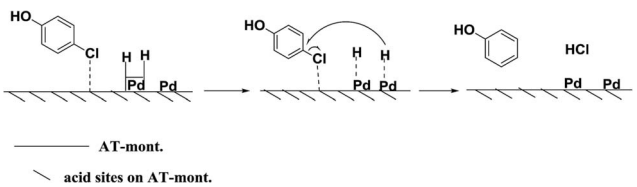

Scheme 1 A possible reaction pathway for the catalytic HDC of 4-CP on PdNP@AT-mont.

higher temperature. This is because, with increase in particle sizes, the solubility of hydrogen increases thereby leading to forward reaction. However, at lower temperature the conversion was slow because the reaction equilibrium reaches fast for the formation of HCl as by-product. Also the generated HCl may poisoned the Pd NPs and thereby reducing its efficiency.[49,50] With the increase of temperature, enhancement of rate was observed *i.e.* shifting the reaction equilibrium occurs to forward direction. In the present study, the reactions were performed in six different temperatures with different time period [Fig. 7(a)]. The best result was found at reaction temperature of 80 °C with 3 h reaction time and showed a conversion up to 97%. The rate constant for the pseudo first order rate of HDC of 4-CP (80 °C) is determined by the method of linear regression [Fig. 7(b)]. The pseudo first order rate constants was found to be 0.019 min^{-1} calculated from the slope of the plot of $\ln(A_0/A_t)$ *versus* time, where A_0 is the initial concentration and A_t is the concentration at time with the r^2 value 0.983 which indicates first order kinetics.

The catalyst recyclability was investigated for the HDC of 4-CP at 80 °C. The catalyst was separated from the reaction mixture after every reaction by simple filtration and then washed with acetone, followed by drying in a desiccator and reused in fresh reaction and the process of recycling was repeated up to fifth run. It was observed that the recycled catalyst remained active without any significant loss in efficiency [Fig. 8].

The possible change of morphology of the recovered catalyst was further investigated through N_2-sorption analysis. A decrease in the BET surface area of the recovered catalyst was found to a certain extent from that of the fresh catalyst [Table 1]. The BJH pore size and pore volume of the recovered catalysts after 5th run remained same [ESI Fig. 5†]. The decrease in the BET surface area after the reactions may be due to clogging of some pores. To check the heterogeneity of the catalyst, hot filtration test was also performed for HDC of 4-CP at 80 °C, in which the reaction was allowed to run for two hour and then the catalyst was separated from the reaction mixture and it was allowed to run without the catalyst for next three hours. The conversion before separation of the catalyst remained unchanged after its removal, which indicates that no leaching of any active species of the catalyst took place.

A possible reaction pathway for the HDC of 4-CP in presence of Pd NPs supported on AT-mont. and molecular hydrogen is shown in Scheme 1. The acid sites present in the support may be responsible for the attachment of the Cl atom of 4-CP leading to the initiation of the reaction.[42,49] A comparison of different reported catalysts for HDC with the present catalyst is shown in Table 3. It is observed that the present catalyst is found good to better in comparison to the other catalysts excluding the temperature factor which is almost comparable.

4. Conclusion

PdNP@AT-mont. catalyst has been synthesized by a green biosynthesis process where Pd NPs generated *in situ* into the nanopores of modified montmorillonite. It was characterized using PXRD, TEM, SEM-EDX, XPS, TPR and surface area analysis. The catalyst showed efficient activity for hydrodechlorination of hazardous 4-chloro phenol in water under base free condition with 100% selectivity and maximum conversion up to 98%. The catalyst was recovered by simple filtration and recycled for five

Table 3 Comparison of the present catalyst with some of the reported catalyst for HDC of 4-CP

Sl no.	Catalyst	Solvent	Base	Temperature (°C)	Time (h)	Conversion/yield (%)
1	$AgPd_4$ supported on carbon[49]	THF	NaOH	25	4	99
2	Pd/C[51]	H_2O	HCOONa	RT	3	100
3	Pd/AC with modified active carbon support[52]	H_2O	Not used	75	Not clearly mentioned	>95
4	Pd/clay[53]	H_2O	Not used	Not clearly mentioned	5	~25
5	PdNP@AT-mont. (present work)	H_2O	Not used	80	3	97

runs without any significant loss of efficiency. The simple green process, easy recovery and operational simplicity with green reaction condition are the advantages of the synthesized catalyst.

Acknowledgements

The authors are grateful to Dr D. Ramaiah, Director, CSIR-North East Institute of Science and Technology, Jorhat-785006, Assam, India for his kind permission to publish the work. The authors thank Dr P. Sengupta, Head, Materials Sciences and Technology Division, CSIR-NEIST, Jorhat, for his constant encouragement. Thanks to CSIR, New Delhi [Project No. CSC-0125, CSC-0135 and BSC-0112] for the financial support. The authors P. K. Saikia and R. P. Bhattacharjee thankful to CSIR, New Delhi for providing the fellowship under Project No. CSC-0135 and BSC-0112 respectively.

References

1 P. Michler, A. Imamoglu, M. D. Mason, P. J. Carson, G. F. Strouse and S. K. Buratto, *Nature*, 2000, **406**, 968–970.
2 C. N. R. Rao, G. U. Kulkarni, P. J. Thomas and P. P. Edwards, *Chem. Soc. Rev.*, 2000, **29**, 27–35.
3 *Metal Nanoparticles: Synthesis, Characterization and Application*, ed. D. L. Feldheim and C. A. Floss Jr, CRC Press, New York, 2002.
4 K. Jacobs, D. Zaziski, E. C. Scher, A. B. Herhold and A. P. Alivisatos, *Science*, 2001, **293**, 1803–1806.
5 A. C. Templeton, W. P. Wuelfing and R. W. Murray, *Acc. Chem. Res.*, 2000, **33**, 27–36.
6 S.-W. Kim, J. Park, Y. Jang, Y. Chung, S. Hwang, T. Hyeon and Y. W. Kim, *Nano Lett.*, 2003, **3**, 1289–1291.
7 G. Schmid and B. Corain, *Eur. J. Inorg. Chem.*, 2003, 3081–3098.
8 B. J. Borah, D. Dutta and D. K. Dutta, *Appl. Clay Sci.*, 2010, **49**, 317–323.
9 J. D. Aiken and R. G. Finke, *J. Am. Chem. Soc.*, 1999, **121**, 8803–8810.
10 F. Schröder, D. Esken, M. Cokoja, M. W. E. van den Berg, O. I. Lebedev, G. V. Tendeloo, B. Walaszek, G. Buntkowsky, H. H. Limbach, B. Chaudret and R. A. Fischer, *J. Am. Chem. Soc.*, 2008, **130**, 6119–6130.
11 T. Tsukatani and H. Fujihara, *Langmuir*, 2005, **21**, 12093–12095.
12 A. Phukan, J. N. Ganguli and D. K. Dutta, *J. Mol. Catal. A: Chem.*, 2003, **202**, 279–287.
13 O. S. Ahmed and D. K. Dutta, *Langmuir*, 2003, **19**, 5540–5541.
14 Y. Wang, J. Yao, H. Li, D. Su and M. Antonietti, *J. Am. Chem. Soc.*, 2011, **133**, 2362–2365.
15 P. B. Malla, P. Ravindranathan, S. Komarneni and R. Roy, *Nature*, 1991, **351**, 555–557.
16 B. J. Borah, D. Dutta, P. P. Saikia, N. C. Barua and D. K. Dutta, *Green Chem.*, 2011, **13**, 3453–3460.
17 P. K. Saikia, P. P. Sarmah, B. J. Borah, L. Saikia, K. Saikia and D. K. Dutta, *Green Chem.*, 2016, **18**, 2843–2850.
18 P. P. Sarmah and D. K. Dutta, *Green Chem.*, 2012, **14**, 1086–1093.
19 P. K. Saikia, P. P. Sarmah, B. J. Borah, L. Saikia and D. K. Dutta, *J. Mol. Catal. A: Chem.*, 2016, **412**, 27–33.
20 E. S. Abdel-Halim, M. H. El-Rafie and S. S. Al-Deyab, *Carbohydr. Polym.*, 2011, **85**, 692–697.
21 S. P. Dubey, M. Lahtinen and M. Sillanpa, *Process Biochem.*, 2010, **45**, 1065–1071.
22 G. Zhan, J. Huang, M. Du, I. Abdul-Rauf, Y. Ma and Q. Li, *Mater. Lett.*, 2011, **65**, 2989–2991.
23 X. Huang, H. Wu, S. Pu, W. Zhang, X. Liao and B. Shi, *Green Chem.*, 2011, **13**, 950–957.
24 K. B. Narayanan and N. Sakthivel, *Adv. Colloid Interface Sci.*, 2010, **156**, 1–13.
25 V. Kumar and S. K. Yadav, *J. Chem. Technol. Biotechnol.*, 2009, **84**, 151–157.
26 P. Mohanpuria, N. K. Rana and S. K. Yadav, *J. Nanopart. Res.*, 2008, **10**, 507–517.
27 S. Iravani, *Green Chem.*, 2011, **13**, 2638–2650.
28 S. K. Nune, N. Chanda, R. Shukla, K. Katti, R. R. Kulkarni, S. Thilakavathy, S. Mekapothula, R. Kannan and K. V. Katti, *J. Mater. Chem.*, 2009, **19**, 2912–2920.
29 R. Pandey, P. Chandra, M. Srivastava, D. K. Mishra and B. Kumar, *Phytochem. Anal.*, 20 15, **26**, 383–394.
30 F. L. Hakkim, C. Gowrishankar and S. Girija, *J. Agric. Food Chem.*, 2007, **55**, 9109–9117.
31 A. Nair and M. K. K. Pillai, *Sci. Total Environ.*, 1992, **121**, 145–157.
32 L. J. Graham, J. E. Atwater and G. N. Jovanovic, *AIChE J.*, 2006, **52**, 1083–1093.
33 H. J. Amezquita-Garcia, E. Razo-Flores, F. J. Cervantes and J. R. Rangel-Mendez, *Carbon*, 2013, **55**, 276–284.
34 L. Calvo, M. A. Gilarranz, J. A. Casas, A. F. Mohedano and J. Rodriguez, *J. Hazard. Mater.*, 2009, **161**, 842–847.
35 Z. Jin, X. Wang, S. Wang, D. Li and G. Lu, *Catal. Commun.*, 2009, **10**, 2027–2030.
36 M. A. Keane, *J. Chem. Technol. Biotechnol.*, 2005, **80**, 1211–1222.
37 M. A. Keane, *ChemCatChem*, 2011, **3**, 800–821.
38 J. A. Baeza, L. Calvo, M. A. Gilarranz and J. J. Rodriguez, *Chem. Eng. J.*, 2014, **240**, 271–280.
39 J. A. Baeza, L. Calvo, J. J. Rodriguez, E. Carbó-Argibay, J. Rivas and M. A. Gilarranz, *Appl. Catal., B*, 2015, **168–169**, 283–292.
40 E. Diaz, A. F. Mohedano, J. A. Casas, L. Calvo, M. A. Gilarranz and J. J. Rodriguez, *Appl. Catal., B*, 2011, **106**, 469–475.
41 S. Gómez-Quero, F. Cárdenas-Lizana and M. A. Keane, *Chem. Eng. J.*, 2011, **166**, 1044–1051.
42 J. A. Baeza, L. Calvo, M. A. Gilarranz, A. F. Mohedano, J. A. Casas and J. J. Rodriguez, *J. Catal.*, 2012, **293**, 85–93.
43 A. Azzouz, D. Nistor, D. Miron, A. V. Ursu, T. Sajin, F. Monette, P. Niquette and R. Hausler, *Thermochim. Acta*, 2006, **449**, 27–34.
44 T. T. Isimjan, Q. He, Y. Liu, J. Zhu, R. J. Puddephatt and D. J. Anderson, *ACS Sustainable Chem. Eng.*, 2013, **1**, 381–388.
45 E. Karakhanov, A. Maximov, Y. Kardasheva, V. Semernina, A. Zolotukhina, A. Ivanov, G. Abbott, E. Rosenberg and V. Vinokurov, *ACS Appl. Mater. Interfaces*, 2014, **6**, 8807–8816.
46 A. Aznarez, A. Gil and S. A. Korili, *RSC Adv.*, 2015, **5**, 82296–82309.

47 A. S. Ivanova, E. M. Slavinskaya, R. V. Gulyaev, V. I. Zaikovskii, O. A. Stonkus, I. G. Danilova, L. M. Plyasova, I. A. Polukhina and A. I. Boronin, *Appl. Catal., B*, 2010, **97**, 57–71.
48 P. J. Ferreira, G. J. La O', Y. Shao-Horn, D. Morgan, R. Makharia, S. Kocha and H. A. Gasteiger, *J. Electrochem. Soc.*, 2005, **152**, A2256–A2271.
49 H. Rong, S. Cai, Z. Niu and Y. Li, *ACS Catal.*, 2013, **3**, 1560–1563.
50 M. A. Aramendia, V. Borau, I. M. Garcia, C. Jimenez, F. Lafont, A. Marinas, M. J. Marinas and J. F. Urbano, *J. Mol. Catal. A: Chem.*, 2002, **184**, 237–245.
51 A. Arcadi, G. Cerichelli, M. Chiarini, R. Vico and D. Zorzan, *Eur. J. Org. Chem.*, 2004, **16**, 3404–3407.
52 L. Calvo, M. A. Gilarranz, J. A. Casas, A. F. Mohedano and J. J. Rodriguez, *Appl. Catal., B*, 2006, **67**, 68–76.
53 P. Kar and B. G. Mishra, *J. Cluster Sci.*, 2014, **5**, 1463–1478.